Superfluid high REynolds von Kármán experiment

B. Rousset,[1,2] P. Bonnay,[1,2] P. Diribarne,[1,2] A. Girard,[1,2] J. M. Poncet,[1,2] E. Herbert,[3,4]
J. Salort,[5] C. Baudet,[6,7] B. Castaing,[5] L. Chevillard,[5] F. Daviaud,[4] B. Dubrulle,[4]
Y. Gagne,[6,7] M. Gibert,[8,9] B. Hébral,[8,9] Th. Lehner,[10] P.-E. Roche,[8,9] B. Saint-Michel,[4]
and M. Bon Mardion[1,2]

[1]*Université Grenoble Alpes, INAC-SBT, F-38000 Grenoble, France*
[2]*CEA, INAC-SBT, F-38000 Grenoble, France*
[3]*Laboratoire Interdisciplinaire des Énergies de Demain (LIED) – CNRS-UMR 8236, Université Paris Diderot – Sorbonne Paris Cite, Paris, France*
[4]*Laboratoire SPHYNX, CEA/IRAMIS/SPEC, CNRS URA 2464, F-91191 Gif-sur-Yvette, France*
[5]*Laboratoire de Physique de l'ENS de Lyon, CNRS/Université Lyon, F-69364 Lyon cedex 7, France*
[6]*Université Grenoble Alpes, INAC-SBT, F-38041 Grenoble, France*
[7]*CNRS, LEGI, F-38041 Grenoble, France*
[8]*Université Grenoble Alpes, Inst NEEL, F-38042 Grenoble, France*
[9]*CNRS, Inst NEEL, F-38042 Grenoble, France*
[10]*LUTH, Observatoire Paris-Meudon, 5 Pl. Jules Janssen, F-92195 Meudon Cedex, France*

The Superfluid High REynolds von Kármán experiment facility exploits the capacities of a high cooling power refrigerator (400 W at 1.8 K) for a large dimension von Kármán flow (inner diameter 0.78 m), which can work with gaseous or subcooled liquid (He-I or He-II) from room temperature down to 1.6 K. The flow is produced between two counter-rotating or co-rotating disks. The large size of the experiment allows exploration of ultra high Reynolds numbers based on Taylor microscale and rms velocity [S. B. Pope, *Turbulent Flows* (Cambridge University Press, 2000)] ($R_\lambda > 10000$) or resolution of the dissipative scale for lower Re. This article presents the design and first performance of this apparatus. Measurements carried out in the first runs of the facility address the global flow behavior: calorimetric measurement of the dissipation, torque and velocity measurements on the two turbines. Moreover first local measurements (micro-Pitot, hot wire,...) have been installed and are presented. © *2014 AIP Publishing LLC*. [http://dx.doi.org/10.1063/1.4897542]

I. INTRODUCTION

Turbulence is a very important phenomenon for practical purposes, as it governs exchanges at our scale (chemicals and pollutant mixing, stress on structures) when usual fluids are involved (air, water). Put another way, the Reynolds number is large, which means that the fluid inertia widely overcomes the viscous stresses. Very different problems have their origin in turbulence: this diversity originates from a lack of a global understanding of the phenomenon. In comparison, pressure, temperature, and density are sufficient for describing the rest state of a gas, despite the intractable complexity of molecular collisions. A simple hypothesis as molecular chaos does not exist in turbulence. In spite of the apparent disorder, the fluid motion is correlated in a subtle way at all scales. If we could avoid the complete calculation of the velocity field, and replace it with a random sampling having all these correlations, the time saving would be enormous. It would also open the way to a more compact theory (Ref. 1). According to our current knowledge three ranges of scales can be distinguished in a turbulent flow:

- The large scales or forcing scales. They are those where the fluid motion is forced (pipe, jet diameter, fan blade, ...).
- The inertial scales. Forced by the immediately larger scales, they drive the motion of the smaller ones. Viscosity has no influence at this stage. This motion nest-

ing is the origin of the subtle correlations within the velocity field.
- The dissipative scales. Velocity gradients are sufficient at this stage to allow the dissipation of the kinetic energy through the viscosity. This energy, fed at the largest scales, "cascades" along the inertial scales, and is dissipated at the smallest ones. At room temperature, very large scale facilities are needed to produce very large Reynolds numbers, for instance using air,[2,3] or even SF6.[4] Decimeter and meter-sized cryogenic facilities allow to achieve similar, and often larger Reynolds numbers (typically $R_\lambda = 2000$–6000) thanks to the low kinematic viscosity of gaseous[5–7] and (non-superfluid) liquid helium.[8–10]

This paper presents an apparatus for turbulence studies from room temperature down to 1.6 K that combines both advantages. As it is the largest facility to study classical turbulence with liquid helium it reaches a record microscale Reynolds number exceeding $R_\lambda = 10\,000$. Operation with helium up to room temperature will generate flow of much smaller intensity, therefore extending the range Reynolds numbers down to typically $R_\lambda = 1000$.

The construction of the apparatus was motivated by two main scientific objectives. The first is, as explained above, to produce extremely intense classical turbulence in a well-controlled laboratory environment. The second objective is to

explore the turbulence of superfluid helium, in particular by means of local measurements.

Indeed, above a pressure-dependent transition temperature T_λ[11] $\sim$ 2 K, liquid helium behaves like an ordinary fluid. When cooled below T_λ, it undergoes a phase transition from its classical phase (called He-I) to a superfluid phase (He-II). The so-called "quantum turbulence" of He-II has been studied over the last 15 years.[8–10,12–14] In many regards, the understanding of quantum turbulence is still at an infancy stage, in particular around the dissipative length scales.[15,16] A central experimental challenge is to resolve these dissipative scales with local sensors. Although significant progresses have be achieved since the seminal anemometer measurements,[12] the resolution of the smallest superfluid anemometers[17] and vortex probes,[18] around 100–300 μm, remains at least one decade larger than the estimated dissipative scales in all the experiment cited above. The large dimension of the present apparatus allows to bypass this probe limitation by expanding all the characteristic scales of the flow.

To generate the turbulence in the apparatus, we have chosen a von Kármán geometry in which a fluid inside a 0.78 m inner diameter cylindrical tank is stirred by two propellers located at both ends at 0.7 m distance. This setting allows to generate a highly turbulent flow using a human size apparatus and has been extensively characterised and documented during the past twenty years, see, for example, Ref. 19. Moreover, its closed geometry is well adapted to low temperature measurements, as already demonstrated.[12,20,21] Another advantage of the von Kármán flow is its demonstrated flexibility since depending upon the measurement location and forcing conditions it presents either a reasonable example of homogeneous isotropic turbulence, or an interesting case of strong anisotropy. Moreover, depending on the impeller shape and forcing frequency, it may generate rich large scale circulation dynamics or a very stable circulation pattern. It is therefore a laboratory model of many natural flows, the most emblematic being the "VKS" experiment that reproduces many known features of the turbulent geodynamo.[22,23]

To produce a well controlled turbulent flow, covering a wide range of Reynolds numbers, from high to very high ($1000 < R_\lambda < 10\,000$), we will use mainly helium (and its widely adjustable physical properties). As stated above, this new von Kármán cell of unprecedented dimension will either reach higher Reynolds numbers (Re up to 10^8) or to be able to resolve the dissipative scale for lower Re. Furthermore, the apparatus should produce comparable flows both in normal and superfluid helium in order to compare classical and quantum turbulence in similar conditions. Boiling and cavitation would not occur in He-II thanks to the high thermal conductivity of superfluid (cf. van Sciver[24]) but it could occur in He-I unless the flow is pressurised. This motivated the pressurisation of the fluid (up to 4 bars), as also done in Refs. 9, 10, and 14.

In the 1990s, Tabeling and his group[12] have developed a von Kármán flow with helium, gaseous and liquid, both normal and superfluid and reached $R_\lambda \sim 2000$. Using a total head pressure tube, they obtained one of the most cited results on superfluid turbulence. However, the superfluid experiment was limited to dissipation lower than 1 W and the radius of the

cell was limited to 0.04 m. Moreover, this experiment[12] was not pressurized and hot wire anemometry was impossible in normal helium as boiling would have occurred.

To overcome these limitations, we have imposed these criteria for the apparatus design:

- Possibility to control independently pressure and temperature inside the cell in the range [10^2–4×10^5 Pa] and [1.6–300 K].
- Long term temperature and pressure stability insuring reliable calorimetric measurements and statistics.
- Possibility to drive the turbines using speed, torque, or power control.
- Optimized design to allow the simultaneous measurements of various sensors and to minimize the sensor flow disturbance.

In the past, the von Kármán setup has been used to explore both equilibrium properties of swirling turbulence, such as spectra, intermittency, structure functions,[5,25,26] anisotropy and inhomogeneity characterization,[27] and less standard out-of-equilibrium phenomena, such as pressure and power fluctuations.[28,29] More recently, studies have focused on the dynamical properties of the large-scale average structures that have been shown to be prone to intriguing transitions between different flow organisations, resulting in hysteretic cycles,[19,23,30] spontaneous "momentizations" and symmetry breaking,[31–33] zero-mode mechanisms.[34,35] Regarding these transitions, the question is opened, whether the selection mechanisms are totally inertial (infinite Re limit) or if the dissipation and its nature have some influence. One hope is that the Superfluid High REynolds von Kármán (SHREK) experiment can provide insights on that question. Other expected advances in the knowledge of turbulent flows are:

- Universal relations between inertial and dissipative scales, in isotropic and anisotropic flows.
- Influence of the dissipative mechanism, comparing the normal and the superfluid cases.
- Test of the three-dimensional statistical mechanics of turbulence, for the structure of the large scale flow.

The von Kármán apparatus presented hereafter is one of the facilities included in the EuHit European network as the HeJet experiment[9] is.

II. APPARATUS DESCRIPTION

In this experiment, a von Kármán helium flow is produced in a cylindrical cell which is immersed in a large thermostat. This thermostat consists in a cryogenic tank filled with saturated helium cooled permanently by a large refrigerator: the tank is itself hung to a flange which is the upper flange of a cryostat called the "Multipurpose Cryostat." This "Multipurpose Cryostat" is a large cylinder (2.4 m in diameter, 3.95 m in height). Figure 1 shows a sketch of the SHREK experiment, without the Multipurpose cryostat.

A. The von Kármán cell

The von Kármán flow is generated in a cylindrical cell of height 1.16 m and diameter 0.78 m. The flow is generated by
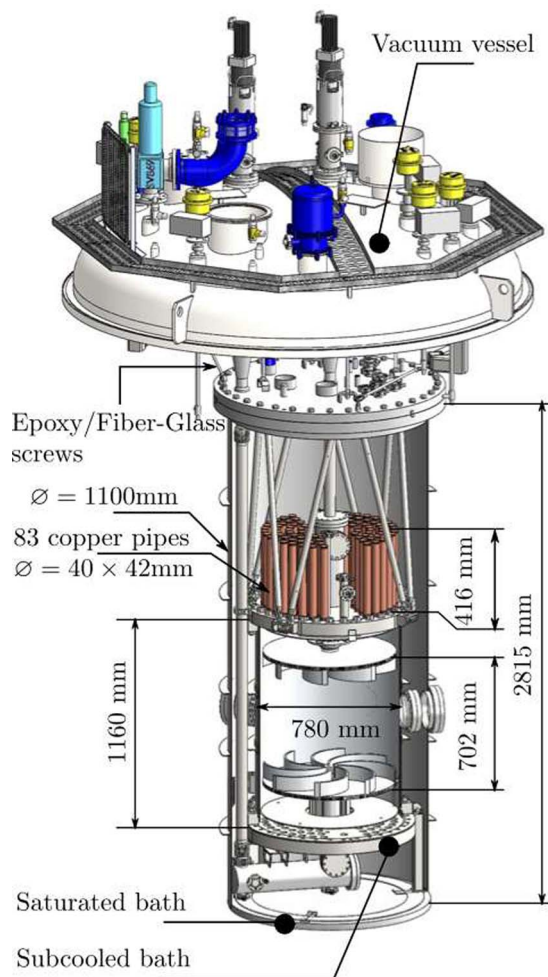
FIG. 1. Sketch of the SHREK experiment with the von Kármán cell (780 mm in diameter), its 83 copper pipes providing heat exchange between the VK cell and the saturated bath enclosed itself in a large tank (1.1 m in diameter, 2.8 m height). The whole assembly is hung to a flange (top of the figure), which is the upper flange of the "Multipurpose cryostat."
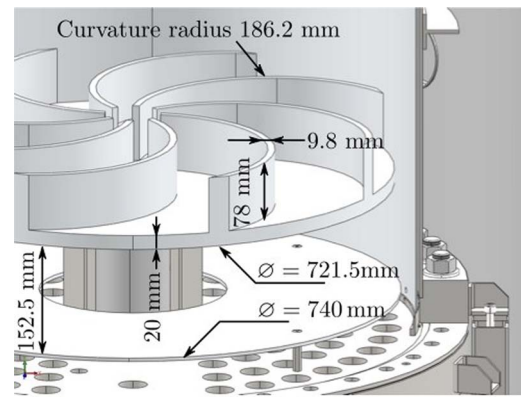

FIG. 2. Geometry of the (lower) impeller and additional aluminium disk below.

symmetry to the apparatus: indeed, at the upper part of the cylinder, 83 cylindrical pipes (described in Sec. II C 1) are welded to the cell, in order to ensure heat exchange between the helium inside the cell and the outer bath (see below); these pipes are present only at the upper part of the cell, and could generate some asymmetries in the flow between upper and lower parts. In order to have the lower parts and upper parts of the cell hydrodynamically comparable, these two disks restore the symmetry of the cell, by "hiding" the heat exchangers to the von Kármán flow. The cylindrical cell (Figure 3) is equipped with 10 radial ports which are intended to provide, in a near future, access for instrumentation, including visualization of the flow. In the experiment presented here the optical ports were not used, and closed with stainless steel

two bladed disks each 0.72 m in diameter (Radius R = 0.36 m). The distance between the inner faces of the two disks is H = 0.7 m, defining an aspect ratio H/R = 1.8, which had been extensively studied in previous and companion experiments using water as a working fluid.[36] The two impellers have 8 curved blades, comparable in shape to those used in VKS1.[37] The dimensions of the von Kármán cell and impellers are in a ratio 4:1 compared to the VKE and 2:1 compared to the VKS experiments.[23] The radius of curvature of the blades is 0.186 m, and the height of the blades is 78 mm (Figure 2). These impellers were entirely machined in an aluminum block with a numerical-control machine tool, which led to a good balance of the impellers.

As the blades of the impellers are not straight, the directions of rotation are no longer equivalent: the (+) direction is defined as the convex part of the blade moves into the fluid, while the (−) is defined as the concave side moves into the fluid. In the SHREK experiment, the two impellers can be rotated independently, in either direction. At a distance of 152 mm upwards/downwards the upper/lower propeller, an extra aluminum disk is added, in order to obtain the best

FIG. 3. The von Kármán experiment with top and bottom flanges, upper and lower propellers (left) and its outer chamber with ports (right). Copper heat exchangers can be seen (upper left).

flanges. In order to keep the best cylindrical symmetry to the present experiments, a 3 mm thick cylindrical aluminum sleeve (0.78 m inner diameter, 1.12 m in height) is inserted in the von Kármán cell to "hide" the ports and provide the best possible R-π symmetry to the cell (for definition of R-π symmetry, see Ref. 30).

The von Kármán cell works with helium cooled at temperatures between 1.6 and 4.5 K, at a pressure which can be adjusted between the mbar range to 4 bars. As superfluid helium operation is the most severe constraint, the cell is therefore designed as a Claudet bath;[38] this decoupling between pressure and temperature avoids cavitation and/or boiling in the von Kármán cell.

B. Mechanical aspects

Moving parts at cold temperature, transmission of movement through vacuum and cryogenic helium, supporting of heavy components, all these different topics raise technical issues which should be addressed in order to ensure a reliable and safe operation of the SHREK experiment.

1. Supporting

The total weight of the SHREK experiment is 3970 kg, including the top flange. A dedicated lifting device has been built, in order to facilitate the handling of the SHREK, as, due to some external constraints, the center of gravity of the SHREK experiment is not located just below the center of the upper flange. The total weight is consequently increased by 400 kg, leading to a total weight of 4370 kg. The tank of the saturated bath is supported with four glass fiber rods 16 mm in diameter; moreover, four additional glass fiber rods have been placed in a quasi horizontal plane. These epoxy glass fiber rods optimize the trade off between mechanical and thermal constraints.

Supporting the von Kármán cell immersed in the saturated bath is a different problem: both tanks are at cold temperature, so that stainless steel will be used instead of fiber glass for the supporting rods. In order to obtain a precise positioning of the von Kármán cell inside the saturated bath, a specially designed octopod made with stainless steel rods has been installed: it provides the necessary flexibility for the positioning of the von Kármán cell inside the tank with saturated helium, where few space is available. Moreover this octopod prevents any vertical torsion of the cell which could be induced by the propeller torque; due to the limited space available, two people (preferably three) are required to perform this tricky operation.

2. The propeller shaft

In order to use commercially available motors, to reduce heat losses and maximize space available at low temperature, perform room temperature torque measurements, motors have been located at room temperature with a complex dedicated shaft from motors to impellers. Indeed, the rotation must be transmitted from the motors which are located at room tem-

perature, to the impellers which are immersed in subcooled helium, through vacuum and saturated helium, without any leaks and with minimum heat loads. The shaft should also accommodate with differential contraction occurring during cool down and warm up, and be operational at room and cryogenic temperature. Whenever commercially available solutions exist, we have used them, most of the time adapting the components to the cryogenic constraints. However, as technical solutions are often not available commercially, we have designed and assembled many components of the kinematic chain.

The components of the kinematic assembly for each couple motor/impeller are the following:

- A brushless motor, with a power of 1300 W and nominal torque of 2.4 Nm. A speeder gear is used to reduce the rotation speed of the motor in the 0–3 Hz range, and increase consequently the torque. The reduction factor is 32, which is also the multiplication factor for the torque (nominal torque thus obtained: 76.8 Nm).
- Ratchet clutches are used to prevent any damage on the motor in case there is some blocking in the kinematic chain. The value, when this device decouples the motor from the rest of the chain, is fixed to 60 Nm.
- A ferrofluidic rotary feedthrough allows the transition between atmospheric pressure and the vacuum in the multipurpose cryostat. This type of ferrofluidic component is ideally suited to our velocity domain, and requires only a long term maintenance.
- A torque-meter is then inserted on the shaft; this device uses strain gauges located on the shaft. Its range covers from 0 to 50 Nm, which is above the expected torque applied. Four comparable torque-meters were bought for the SHREK experiment. However, only two were installed on SHREK without any modification. Indeed, two other torque-meters have been installed at cryogenic temperature (see below), which imposed some additional constraints. The torque-meters mentioned here are located at room temperature (under vacuum), which did not require any modification.
- The transition between vacuum and low temperature (down to 1.6 K) is achieved by a magnetic rotary feedthrough (Figure 4). This feedthrough is based on magnetic coupling between two permanent magnet assemblies (with alternated north/south poles): this kind of magnetic coupling ensures excellent torque transmission, and it allows to insulate the cold part (possibly filled with superfluid helium) from the vacuum. The insulating part is made with a magnetic stainless steel, and is located in the gap between the two magnetic assemblies. This insulating part is essential to limit heat losses from cold end due to subcooled superfluid heat flux. The permanent magnets used are Nd-FeB magnets with high remnant and coercive fields. The permanent magnetization is only slightly affected by the cold temperature, so that this system has a long time reliability. It was sized (and experimentally verified) to transmit torques up to 85 Nm without mechanical friction. This system, despite interrupting
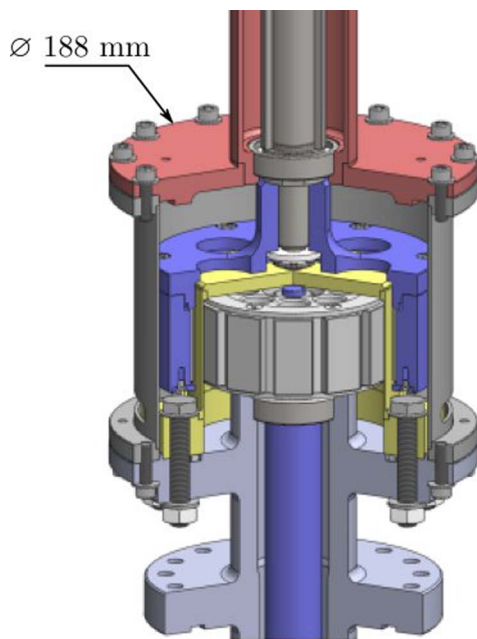
FIG. 4. Magnetic coupler for torque transmission between cold (bottom) and warm (top) ends. Yellow: the part ensuring leaktightness between He-II and vacuum.

the continuity of the shaft, transmits torques with excellent reliability.

- After the magnetic coupler/feedthrough, the length of the shaft is 613 mm for the upper impeller and 2310 mm down to the 90° gear box for the bottom impeller. To take into account the contraction of stainless steel at low temperature (3.2 mm/m from room temperature to 4 K), a splined shaft is used.
- A cold torque-meter is inserted just before the impeller to measure the torque as close as possible to the impeller. This torque-meter has been customized to work at low temperature: aluminum was replaced by stainless steel, the commercial ball bearings are replaced by "hybrid" ball bearings composed of ceramic balls moving in a stainless steel cage. This technique of "hybrid" ball bearing has proved to work satisfactorily.
- After the torque-meter the impeller itself drives the fluid.

For the bottom impeller, two 90° gear boxes are necessary to transmit the rotation.

A schematic of the kinematic chain and its components is shown in Figure 5. All the components of the kinematic chain are tested independently at liquid nitrogen temperature whenever it is possible. The assembly of the various components of SHREK is performed in a dedicated room with adapted material handling tools; for the final assembly of the whole system, the upper flange of SHREK is placed on a dedicated support with 5 m height available below, so that all cryostats can be fixed to the flange before being inserted into the Multipurpose cryostat.

C. Cryogenics: Steady state operation and cool down

In order to achieve the high Reynolds numbers expected in this experiment, a significant amount of energy should be
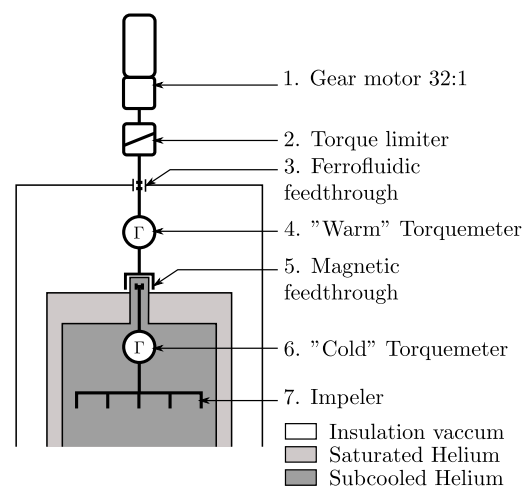

FIG. 5. Schematic of the kinematic chain of the SHREK.

permanently injected. Conversely, this energy needs to be steadily removed from the von Kármán cell. This is achieved *via* a large refrigerator available in the laboratory.

1. Description of the process

The cooling system is based on the refrigerator available at SBT.[39] This facility has been in operation since 2004, when it reached its nominal performances. The refrigeration power available ranges from 120 W at 1.5 K to 800 W at 4.5 K, and the temperature can be adjusted in the range 1.5–4.5 K continuously. A simplified flow scheme of the refrigerator is shown in Figure 6.
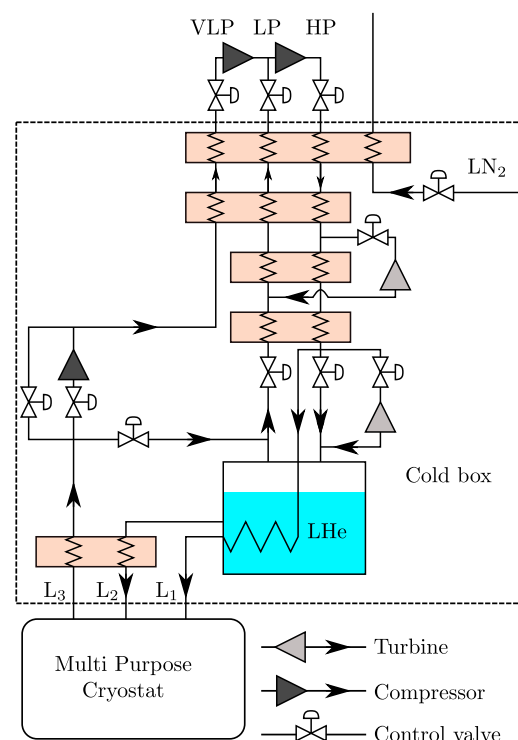

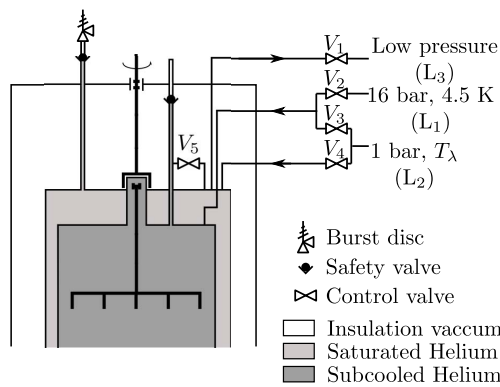FIG. 6. Simplified PFD of the refrigerator. The three cryolines to SHREK are shown (bottom left).

FIG. 7. SHREK simplified flow diagram.

The cooling power available in the refrigerator is transferred to the experiments through a cryogenic line from the refrigerator to the Multipurpose Cryostat, where the SHREK experiment is inserted. Three cryolines are connected to the SHREK experiment (Figures 6 and 7): L_1 the High Pressure (HP, 16 bars), 4.5 K line coming from the cycle gas is cooled through the LHe bath of the refrigerator: this line is equipped with the V2 valve (Figure 7); L_2 the so called (1 bar, T_λ) line, coming from the LHe bath of the refrigerator and exchanging with the return line through the heat exchanger (Figure 6, bottom left) is equipped with two valves V3 and V4 (Figure 7); L_3 the low vapor pressure return line, flowing back to the refrigerator is equipped with valve V1 (Figure 7). In steady state, only the V4 and the V1 valves are open: the pressure in the saturated helium bath, and consequently the temperature, is fixed according to the adjustment of the speed of the cold compressor of the refrigerator. In order to have the lowest temperature of the von Kármán cell, it is equipped at the top of its flange with 83 tubular copper heat exchangers: these tubes have a thickness of 1.6 mm and inner diameter of 40 mm. They are 0.4 m long, providing an equivalent exchange surface of 4 m^2 between the cell and the saturated bath. The bottom extremity of these tubes is welded by electron beam around a stainless steel pipe, which is itself TIG welded on the upper flange of the von Kármán cell. Taking into account the Kapitza resistance, the thermal conductivity of the standard copper used, the temperature difference between the von Kármán cell and the saturated bath is estimated to a few tens of milliKelvins in the range 1.5–2.1 K (in the superfluid operation of SHREK).

2. Safety issues

All vessels were built according to the ASME safety regulation. The saturated bath has been designed to withstand a maximum inner pressure of 5 bars, which means a pressure difference of 4 bars between the tank and atmospheric pressure. The saturated bath is at subatmospheric pressure, when temperatures below 4.2 K are needed; this bath is inside the Multipurpose Cryostat, which is under vacuum. The most severe accident is the loss of vacuum, and the subsequent heat inlet to the saturated bath. To minimize this flux, 30 layers of Multi Layer Insulator (MLI) have been installed around the

FIG. 8. Insertion of the saturated bath (covered with MLI) into the Multipurpose cryostat.

saturated bath (Figure 8). This MLI has also the advantage to reduce radiative heat loads. To protect the saturated bath against overpressure, a safety valve with helium guard and in series a burst disk to ambient atmosphere have been installed to minimize the weight of the safety devices (Figure 7). For the von Kármán cell, two safety valves in series have been installed for protection against overpressure: a home made cold safety valve allows the transition between the temperature of superfluid helium and normal helium. A second safety valve in series is located at room temperature to avoid any leak.

3. Filling and cooling down

SHREK facility and its associated refrigerator are cooled down simultaneously, after pumping of their vacuum chamber and helium conditioning of all inner circuits. Valves V1, V2, and V5 (Figure 7) are open to fill with liquid helium both the von Kármán cell and refrigerator. Supercritical helium coming from refrigerator is discharged through the valves producing a two-phase mixture. After some time, the von Kármán
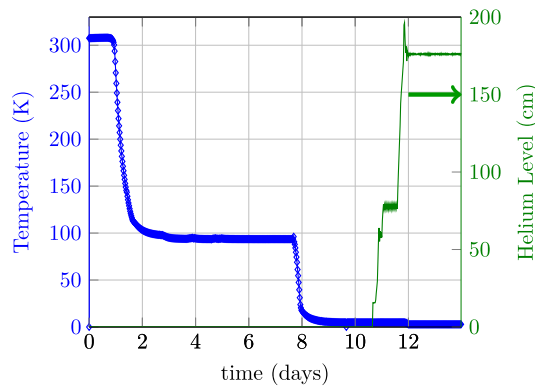
FIG. 9. Cool down. The helium level is measured inside the saturated bath.

cell is filled with a diphasic mixture, where the gas is mostly concentrated at the top of the cell, especially in the tubular heat exchangers. Once the level inside the cold box is above the top of the copper heat exchanger of the von Kármán cell, V2 and V5 valves are closed while V3 valve is opened and V4 valve aperture is controlled by the level of liquid in the saturated bath. The vapor generated inside the saturated bath is pumped through the cold compressor to decrease the temperature of the bath. This temperature should be decreased below superfluid transition, so that the high thermal conductivity of superfluid helium allows fast condensation of the gas still inside the von Kármán cell. Once the copper heat exchanger pipes are completely filled with superfluid, the V3 valve is closed, so the subcooled liquid is in a closed volume. Pressure inside the cell must remain constant after the closure of the V3 valve if the filling is complete (providing the temperature is kept constant). If the filling is performed close to the T_λ line, then any change in temperature (below or above T_λ) of this closed volume induces an increase of pressure (due to the second order transition when crossing the lambda line). Once the filling of the cell is complete, the temperature of the refrigerator is regulated to the desired value by controlling the speed of the cold compressors. A sequence of cool down is shown on Figure 9. Two steps were made at intermediate temperature: at 80 K, and at 10 K during which tests were made of the rotation of the two impellers.

III. SENSORS AND FACILITY CONTROL SYSTEM

A. Measurements in the saturated helium bath

Two Allen-Bradley carbon sensors are located at the top and bottom of the saturated bath; they provide temperature measurements during the runs, while two PT100 platinum resistors at the same place are used during cool down and warm up. Two room temperature pressure transducers connected to the saturated bath can also be used to calculate the temperature at saturation. The liquid level in the tank is monitored thanks to a superconductive gauge. Measurements of mass flow rates coming into and out of the saturated bath are provided by respectively Coriolis and Venturi flowmeters. A resistive heater with 4 wire measurement is also placed below the von Kármán cell: this heater is used to make the warm up

procedure faster as well as to calibrate the von Kármán heat exchanger (see Sec. IV B).

B. Measurements in the von Kármán cell

Two cernox sensors located at the bottom and the top of the cell (between the turbines and the flanges) allow temperature measurements from room temperature down to 1.5 K. The pressure in the cell is measured with a pressure gauge located at room temperature connected to the cell via a capillary pipe (used to minimize heat loss due to superfluid critical heat flux). Resistive heaters glued on the back side of the aluminum horizontal plates are used to perform differential calorimetric measurements (see below). As mentioned above, the outer vessel is equipped with viewports which can be used to insert sensors directly inside the flow generated by the turbine, or, in the future, for visualization of the flow. The angular velocity of the turbines is currently measured at the motor level, but a more accurate high frequency velocity measurement at the turbine location has also been implemented. Customized cryogenic and classical room temperature torque-meters are inserted along the propeller shaft: this redundancy has been installed, to ensure torque measurements even in case of failure of cryogenic torque-meters. Indeed, torque-meters at low temperature are expected to measure the torque on the impellers with more precision than warm torque-meters (as these torque-meters are more subject to noise and offsets).

C. Control system and data acquisition

The SHREK experiment is connected to the 400 W refrigerator through the Multipurpose cryostat and the cryogenic line. Its control system is therefore interfaced with the already existing control system of the 400 W: the refrigerator is controlled through three Programmable Logical Controllers (PLC) which control 40 analogical actuators (valves, heaters), 120 logical actuators. Ninety different temperatures are measured, together with 40 pressure measurements. Twenty regulation loops are necessary to ensure proper and flexible operation of the refrigerator. The Multipurpose cryostat is controlled by its PLC which ensures the control of the quality of vacuum and interfaces with the refrigerator (valves, flow rate). The SHREK experiment is controlled via its PLC, which controls 12 analogical actuators (ten valves and two heaters), the two controllers dedicated to the brushless motors. The PLC of the whole installation (Refrigerator + Multipurpose Cryostat + SHREK) are interconnected through an Ethernet Modbus TCP field network and are connected to the three Supervisory Control and Data Acquisition (SCADA), which are used for monitoring, control, and data acquisition.

To go into more details, the following functions have been implemented in the PLC: (i) Safety: management of the installation, in particular in case of overpressure in the system; (ii) Operation: different operation modes are identified as cool down, night operation (reduced mode), nominal operation, and data acquisition. The regulation loops are activated on request according to the operating mode requested.

(iii) Management of the impellers: different regulation loops are implemented. The rotation frequency of each impeller (f1, f2 the frequencies of the upper and lower turbines, respectively) can be regulated separately or a special regulation procedure can be used, with two other control parameters: the rotation frequency of the upper turbine f1 and the rotation number θ, or possibly the "mean angular frequency" ω and rotation number θ being defined as

$$\theta = \frac{f_1 - f_2}{f_1 + f} \quad \omega = 2\pi \frac{f_1 + f_2}{2} = \frac{\omega_1 + \omega_2}{2}. \quad (1)$$

Data are usually acquired in the control system at a rate of 1 Hz, while data related to the measurement of the turbulent flow (speed of the impeller, torquemeters, hot wire) use a fast acquisition system (PI-3920 data acquisition device).

IV. EXPERIMENTAL RESULTS

A. Control parameters

The experimental control parameters are the temperature of the fluid and the pressure in the cell. Moreover, the flow is governed by the value of the frequencies of rotation of the turbines, or possibly by the value of one frequency and the value of θ, or also possibly the couple (ω, θ). The long term stability of the temperature in the von Kármán cell has been verified to be less than 1 mK in superfluid helium, which ensures constant fluid properties throughout the experiment. The satisfactory thermal operation of the SHREK experiment is strongly related to the efficiency of the heat exchangers installed on the upper part of the von Kármán cell. Indeed, the temperature difference between the saturated bath and the von Kármán cell is very low (Figure 10). This temperature difference fully agrees with calculations (see Sec. IV C 1). Figure 10 has been established as a calibration tool for calorimetric measurements: once the maximum power available at the working temperature has been injected in the heater immersed in the saturated bath, and a stable temperature achieved in the von Kármán cell, the heater inside the cell is energized to inject power step by step. In the meantime, same power step is removed from the heater of the saturated bath, so the overall power is maintained. This power $\dot{Q}$ injected in
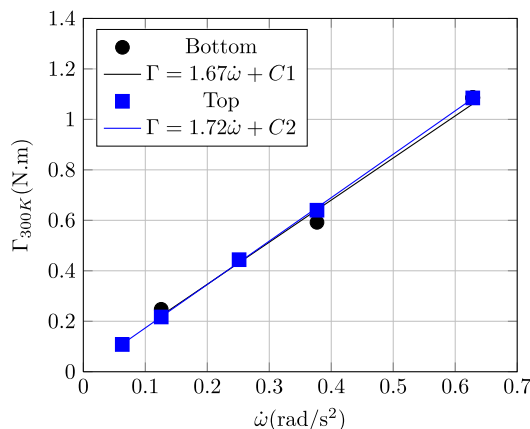

FIG. 10. Temperature difference between the von Kármán cell and the saturated bath.

the von Kármán cell is evacuated via the heat exchangers, and leads to a certain temperature difference ΔT between the von Kármán cell and the saturated bath according to the following equation:

$$\dot{Q} = \Delta T \ K(T). \quad (2)$$

This procedure was performed at different He-II temperatures. Slopes of curves of applied powers versus temperature differences give access to the overall heat exchange coefficient $K(T) = \frac{\dot{Q}}{\Delta T}$.

This calibration is thus available for calorimetric measurements (e.g., turbine dissipation).

It is worth noticing that due to the very large thermal conductivity of He-II, the whole cell (including dead volumes where thermometers and heat exchanger are located) is isothermal. For the same reason the diffusion time is quite small and the thermal transients are short.

B. Room temperature measurements

Before cool down some preliminary measurements were performed, with impellers in rotation in helium gas at room temperature; as the density of helium is much lower at 300 K than at low temperature, the values of torques are much lower. The two torque-meters installed on each shaft (warm and cold torque-meter) are verified to lead to very similar results.

Torque measurements performed with helium at room temperature at different constant rotation speeds allow to calculate the "static" friction torque; they exhibit a linear dependency with the frequency, which most probably comes from eddy currents present in the magnetic rotating feedthrough.

The moment of inertia of the impellers have been measured as follows: according to Newton's law (see Eq. (3)), the time derivative of the angular momentum I ω (I the moment of inertia of the turbine) is equal to the sum of torques; one obtains

$$I \dot{\omega} = \Gamma_{300K} - \Gamma_{static} - \Gamma_{eddy\_current} - \Gamma_{fluid}, \quad (3)$$

where Γ_{300K} is the torque measurement at room temperature, Γ_{static} is the torque associated to the solid friction losses (bearing, gear boxes,…), $\Gamma_{eddy\_current}$ is the contribution of the eddy current induced in the magnetic coupler (relevant only for the ambient torque measurement), and Γ_{fluid} is the torque corresponding to the flow induced by the turbine. This latter term is negligible for helium gas at room temperature and atmospheric pressure. Γ_{static} does not depend on angular velocity, and we will show in the following that its value is very low. Finally for sufficient angular acceleration, $\Gamma_{eddy\_current}$ can be neglected. Once the turbine is energized at a constant slow speed (i.e., with low eddy currents), different constant angular accelerations of turbine are imposed via the control system and the corresponding torques are recorded. Each point is performed between 0.1 and 1 Hz, with different speed rates. The slope of the curve "torque versus angular acceleration" leads to the moment of inertia (Figure 11). The values thus derived are in excellent agreement with the computations derived from CAD design outputs.
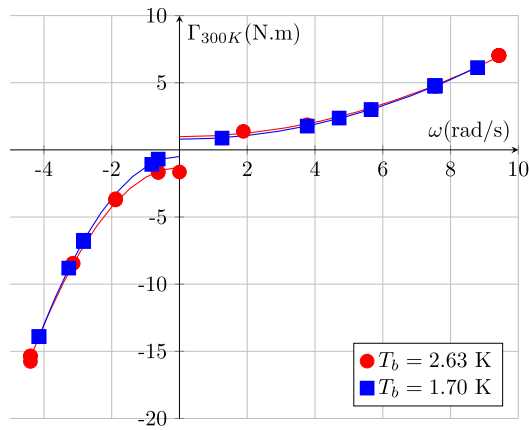
FIG. 11. Torque versus acceleration: measurements of the moment of inertia (fluid at 300 K).

C. Measurements at low temperature

1. Torques

Torques measured at low temperature are larger than at room temperature, as already mentioned. Figure 12 shows torque measurements at 1.63 K and at 1.1 bar in the cell.

The torque measured at room temperature is non-zero at rest, due to "static" torques in the kinematic assembly (bearing, gear boxes and magnetic feedthroughs). The torques in both directions are different in values, but show both a parabolic behavior: this behavior is typical for turbulent flow in the cell; for positive values of rotation, the torques are lower than in the other direction. In positive direction, the velocity of the fluid at the exit of the blades is oriented for an efficient pump work, which is the inverse in reverse direction. The values of torques are fully consistent with calorimetric measurements which have been performed independently: as an example at 1.4 Hz in the positive direction, the torque is 6.1 Nm including 0.75 Nm for the static torque. The power associated with the two impellers is 107 W, in very good agreement with the 106 W obtained with the calorimetric measurements. The corresponding Reynolds number (based on the radius of the cell, the viscosity of the normal component, and the total density) is 7×10^7, which is two orders of magnitude higher than the Reynolds numbers obtained in water with the homothetic
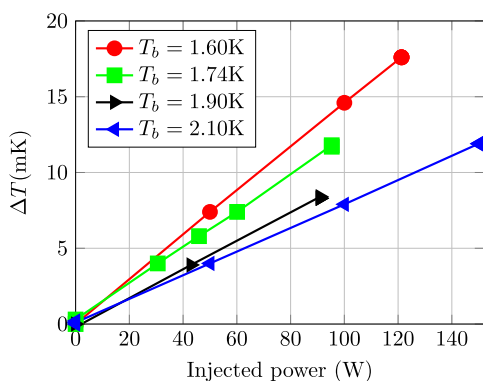

FIG. 12. Torque measurement (300 K torque-meter) versus frequency of rotation for two temperatures in the von Karman cell.

experiment already mentioned.[19,30] As, for a given Reynolds the dissipation varies linearly with density and third power of the inverse of the kinematic viscosity, it would be necessary to extract respectively 80 MW and 400 MW to reach the same Re in water or air at STP in an von Kármán cell of identical dimensions. This illustrates the technological interest to work with cryogenic helium.

2. Power dissipation in the flow $\dot{Q}_{flow}$

Power dissipation in the flow $\dot{Q}_{flow}$ can be estimated through the calibration performed (i.e., using Eq. (2) and Figure 10), and taking into account static torques. However, a small part of the total power $\dot{Q}$ in (2) is due to "static" torques and has to be removed to calculate the dissipation due to the von Kármán flow only leading to the following equation:

$$\dot{Q}_{flow} = \Delta T \, K_{(T)} - \Gamma_{static\_1}\omega_1 - \Gamma_{static\_2}\omega_2. \qquad (4)$$

The values of Γ_{static_1} and Γ_{static_2} are taken equal to the "static" torques measured by the room temperature torquemeters, as all the power dissipated inside the vacuum vessel will be removed in the von Kármán cell through the high conductive subcooled supefluid path. In Eq. (4) as in Eq. (3) again, the torque associated to the magnetic coupler are neglected, which is valid at moderate frequency.

The ratio of this power dissipated in the fluid divided by the mass M present between the turbines expresses the dissipation rate. This dissipation rate is reduced to a non-dimensional number according to the classical equation:[40]

$$\langle \varepsilon_D \rangle^* = \frac{\dot{Q}_{flow}}{M \, R^2 \, \omega^3} = \frac{\dot{Q}_{flow}}{\rho \, \pi \, R^4 \, H \, \omega^3}. \qquad (5)$$

Therefore, measurements of Q_{flow} give access to dissipation in the fluid.

On the other hand, it is interesting to evaluate the power injected in the flow. As torque and rotation frequency were acquired for each turbine, and using the same dimensionless approach, it is straightforward to calculate this input power in the flow as

$$\langle \varepsilon_i \rangle^* = \frac{\Gamma_1 \, \omega_1 + \Gamma_2 \, \omega_2}{M \, R^2 \, \omega^3} = \frac{\Gamma_1 \, \omega_1 + \Gamma_2 \, \omega_2}{\rho \, \pi \, R^4 \, H \, \omega^3}, \qquad (6)$$

where Γ_1 and Γ_2 are the "hydraulic net torques" (static friction torques being removed).

In steady state, the dissipated power and the injected power should be equal: this can checked by comparing the results given by Eqs. (5) and (6), Figure 13 shows this comparison, as turbines were driven independently, at a mean frequency of 0.45 Hz, the parameter being varied between -1 and $+1$; the temperature of the fluid was 1.63 K (superfluid helium). The very good agreement between measured dissipated and injected powers proves the excellent quality of our measurements.

Moreover, Figure 13 presents features comparable to earlier experiments performed in water.[19,30] It indicates that behavior of the flow in He-II is similar to that of a classical fluid and may be explained by the coupling between the normal and the superfluid component. To proceed further, we should derive a few orders of magnitude. An estimate of the viscous
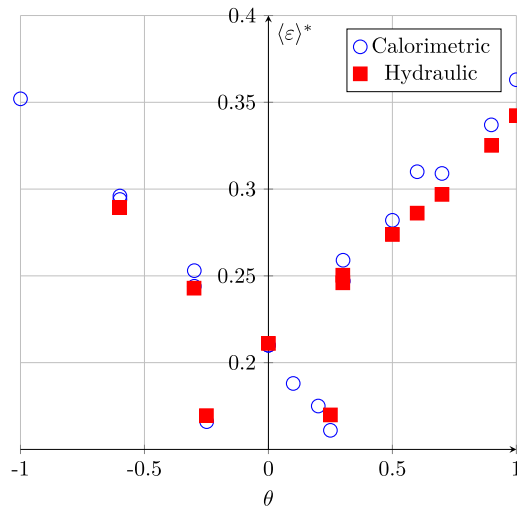
FIG. 13. Calorimetric (empty circles) and hydraulic (squares) power measurements.

dissipative scale can be inferred from the dissipation rate using Eq. (7):

$$\eta = \left[\frac{\upsilon^3}{\langle \varepsilon \rangle} \right]^{\frac{1}{4}}, \qquad (7)$$

where the denominator is the dissipation and $\upsilon = \frac{\mu_N}{\rho}$, μ_N being the dynamic viscosity of the normal component and ρ the total density of the fluid.

From Figure 13 we derive $\langle \varepsilon \rangle \approx 0.7$ W/kg which in turn gives $\eta \sim 1$ μm. Quantum effects are expected below the intervortex distance δ, which can be taken as[41]

$$\frac{\delta}{L} \approx 0.5 \, \mathrm{Re}_\kappa^{-\frac{3}{4}},$$

where L is the integral scale (taken here as the radius of the turbine R), Re_κ is the Reynolds number based on the quantum of vorticity $\kappa = 2\pi \, h/m$:

$$\mathrm{Re}_K = \frac{L \, v_{rms}}{K}.$$

The dissipation rate can provide an estimate of v_{rms}:

$$\epsilon = \frac{(v_{rms})^3}{L}.$$

Taking L = R = 0.4 m and $\varepsilon \sim 0.7$ W/kg, we obtain $v_{rms} \sim 0.7$ m/s, then $\mathrm{Re}_\kappa = 4.5 \times 10^5$, leading to $\delta \sim 10$ μm $> \eta$.

This very simple calculation shows that, up to scales of the order of 10 μm, no difference between superfluid and normal helium can be observed in our experiments, where small scales are not so far analyzed. Indeed, below 10 μm, we could expect to see differences between He-I and He-II. Unfortunately, sensors enabling this resolution are so far not available in SHREK, but these basic calculations explain, why we aim to build such very small scale sensors.

It is also possible to have an estimate of the R_λ based on Taylor scale λ, taking into account the viscosity of helium as above (namely, the dynamic viscosity of normal helium divided by the total density): λ can be estimated from the dissipation rate, thus leading to R_λ through the following equa-

tions:

$$\epsilon = \frac{15 \, \upsilon \, v_{rms}^2}{\lambda^2}, \qquad R_\lambda = \frac{v_{rms}\lambda}{\upsilon}.$$

Leading to $R_\lambda = 20000$.

These orders of magnitude show all the interest of our large facility, and its capability to reach unsurpassed values of Reynolds in well controlled laboratory conditions.

3. Preliminary velocity spectra measurements

Preliminary velocity spectra measurements have been obtained with two anemometers of millimeter size: a Pitot tube and a hot film. There are presented here to illustrate that such low-resolution probes are able to resolve velocity fluctuations over three-decade of frequency bandwidth.

Both probes are positioned at mid-height in the cell, 4 cm (Pitot tube) and 1 cm (hot film) away from the sidewall. Both are pointing in the equatorial direction.

Figure 14 presents the power spectra obtained at 2.55 K with both propellers turning in the same direction at rate 1.23 and 1.55 Hz, that is a mean velocity at the tip of the impellers of 3.5 m/s.[42] The peak near 0.75 Hz is interpreted has a secondary flow resulting for the difference in rotational speed, as supported by measurements at different speeds. Beyond roughly 10 Hz, the spectra exhibit a strong decrease consistent with the turbulent cascade. As expected in such von Kármán flow,[43] the decrease is not as strong as the Kolmogorov dependence $f^{-5/3}$ found in homogeneous isotropic turbulence. The peaks around 100 Hz in the Pitot tube signal are interpreted as an artifact due to mechanical vibrations altering the transducer's operation. The high frequency cut-off of both signals results from limitation in resolution and not from a hydrodynamic cut-off. Thanks to the large dimension of this flow, the very large Reynolds number that can be generated, and knowing that cryogenic hot wire anemometers with effective resolution around 0.01 mm have been operated in smaller flow,[6] the experiment offers the prospect to resolve turbulent fluctuations with a frequency bandwidth exceeding 5 decades.
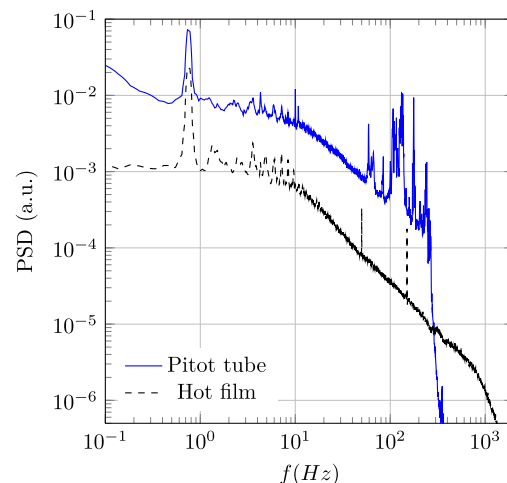

FIG. 14. Velocity power spectra in co-current von Kármán configuration.

V. CONCLUSIONS

A superfluid high Reynolds von Kármán experiment has been designed, manufactured, assembled, and tested. The cell, optimized for subcooled superfluid runs can also work with normal or gaseous helium. Major technological challenges solved involved safety issues, large impeller driving and heat removal in subcooled superfluid conditions. The largest Re numbers ever achieved in a von Kármán cell have been obtained both in normal and superfluid conditions. Torque measurements in these conditions are consistent with those performed in water cells of similar aspect ratio for which the Reynolds number is far smaller (two orders of magnitude smaller than SHREK).

[1] S. B. Pope, *Turbulent Flows* (Cambridge University Press, 2000).
[2] M. V. Zagarola and A. J. Smits, J. Fluid Mech. **373**, 33 (1998).
[3] J.-D. Rüedi, A. Talamelli, H. M. Nagib, P. H. Alfredsson, and P. A. Monkewitz, in *Prog. Turbul. III*, edited by J. Peinke, M. Oberlack, and A. Talamelli (Springer, Berlin, 2010), pp. 73–77.
[4] G. P. Bewley, H. Nobach, M. Sinhuber, H. Xu, and E. Bodenschatz, e-print arXiv:14014970 (2014).
[5] F. Moisy, P. Tabeling, and H. Willaime, Phys. Rev. Lett. **82**, 3994 (1999).
[6] O. Chanal, B. Chabaud, B. Castaing, and B. Hébral, Eur. Phys. J. B: Condens. Matter Complex Syst. **17**, 309 (2000).
[7] S. Pietropinto, C. Poulain, C. Baudet, B. Castaing, B. Chabaud, Y. Gagne, B. Hébral, Y. Ladam, P. Lebrun, O. Pirotte, and P. Roche, Phys. C. Supercond. **386**, 512 (2003).
[8] C. J. Swanson, R. J. Donnelly, and G. G. Ihas, Phys. B. Condens. Matter **284–288**(1), 77 (2000).
[9] D. Duri, C. Baudet, P. Charvin, J. Virone, B. Rousset, J.-M. Poncet, and P. Diribarne, Rev. Sci. Instrum. **82**, 115109 (2011).
[10] J. Salort, B. Chabaud, E. Lévêque, and P.-E. Roche, EPL Europhys. Lett. **97**, 34006 (2012).
[11] The "lambda" subscript is not related to the similar subscript used for the microscale Reynolds number.
[12] J. Maurer and P. Tabeling, EPL Europhys. Lett. **43**, 29 (1998).
[13] S. Fuzier and S. W. Van Sciver, Cryogenics **48**, 130 (2008).
[14] J. Salort, C. Baudet, B. Castaing, B. Chabaud, F. Daviaud, T. Didelot, P. Diribarne, B. Dubrulle, Y. Gagne, F. Gauthier, A. Girard, B. Hébral, B. Rousset, P. Thibault, and P.-E. Roche, Phys. Fluids **22**, 125102 (2010).
[15] W. F. Vinen and J. J. Niemela, J. Low Temp. Phys. **128**, 167 (2002).
[16] L. Skrbek and K. R. Sreenivasan, Phys. Fluids **24**, 011301 (2012).
[17] J. Salort, A. Monfardini, and P.-E. Roche, Rev. Sci. Instrum. **83**, 125002 (2012).
[18] P.-E. Roche, P. Diribarne, T. Didelot, O. Français, L. Rousseau, and H. Willaime, EPL Europhys. Lett. **77**, 66002 (2007).
[19] F. Ravelet, "Bifurcation Globales Hydrodynamiques et Magnetohydrodnamiques Dans Un Écoulement de von Karman Turbulent," École doctorale de l'école Polytechnique, 2005.
[20] G. Zocchi, P. Tabeling, J. Maurer, and H. Willaime, Phys. Rev. E **50**, 3693 (1994).
[21] D. Schmoranzer, M. Rotter, J. Sebek, and L. Skrbek, Experimental setup for probing a von Karman type flow of normal and superfluid helium. Experimental Fluid Mechanics 2009, Proceedings of the International Conference (Technical University of Liberec, Liberec, Czech Republic) (2009), pp 304–309.
[22] M. Berhanu, R. Monchaux, S. Fauve, N. Mordant, F. Pétrélis, A. Chiffaudel, F. Daviaud, B. Dubrulle, L. Marié, F. Ravelet, M. Bourgoin, P. Odier, J.-F. Pinton, and R. Volk, EPL Europhys. Lett. **77**, 59001 (2007).
[23] R. Monchaux, M. Berhanu, M. Bourgoin, M. Moulin, P. Odier, J.-F. Pinton, R. Volk, S. Fauve, N. Mordant, F. Pétrélis, A. Chiffaudel, F. Daviaud, B. Dubrulle, C. Gasquet, L. Marié, and F. Ravelet, Phys. Rev. Lett. **98**, 044502 (2007).
[24] S. W. V. Sciver, *Helium Cryogenics* (Springer, 2011).
[25] F. Moisy, H. Willaime, J. Andersen, and P. Tabeling, Phys. Rev. Lett. **86**, 4827 (2001).
[26] C. Herbert, B. Dubrulle, P. H. Chavanis, and D. Paillard, Phys. Rev. E **85**, 056304 (2012).
[27] P.-P. Cortet, P. Diribarne, R. Monchaux, A. Chiffaudel, F. Daviaud, and B. Dubrulle, Phys. Fluids **21**, 025104 (2009).
[28] S. Fauve, C. Laroche, and B. Castaing, J. Phys. II **3**, 271 (1993).
[29] R. Labbe, J.-F. Pinton, and S. Fauve, J. Phys. II **6**, 1099 (1996).
[30] F. Ravelet, L. Marié, A. Chiffaudel, and F. Daviaud, Phys. Rev. Lett. **93**, 164501 (2004).
[31] A. de la Torre and J. Burguete, Phys. Rev. Lett. **99**, 054101 (2007).
[32] P.-P. Cortet, A. Chiffaudel, F. Daviaud, and B. Dubrulle, Phys. Rev. Lett. **105**, 214501 (2010).
[33] P.-P. Cortet, E. Herbert, A. Chiffaudel, F. Daviaud, B. Dubrulle, and V. Padilla, J. Stat. Mech. Theory Exp. **2011**, P07012 (2011).
[34] B. Saint-Michel, B. Dubrulle, L. Marié, F. Ravelet, and F. Daviaud, Phys. Rev. Lett. **111**, 234502 (2013).
[35] J. Burguete and A. D. L. Torre, Int. J. Bifurc. Chaos **19**, 2695 (2009).
[36] F. Ravelet, A. Chiffaudel, and F. Daviaud, J. Fluid Mech. **601**, 339 (2008).
[37] M. Bourgoin, L. Marié, F. Pétrélis, C. Gasquet, A. Guigon, J.-B. Luciani, M. Moulin, F. Namer, J. Burguete, A. Chiffaudel, F. Daviaud, S. Fauve, P. Odier, and J.-F. Pinton, Phys. Fluids **14**, 3046 (2002).
[38] G. Bon Mardion, G. Claudet, P. Seyfert, and J. Verdier, in *Advances in Cryogenic Engineering*, edited by K. D. Timmerhaus (Springer, US, 1978), pp. 358–362.
[39] P. Roussel, A. Girard, B. Jager, B. Rousset, P. Bonnay, F. Millet, and P. Gully, AIP Conf. Proc. **823**, 1420 (2006).
[40] O. Cadot, Y. Couder, A. Daerr, S. Douady, and A. Tsinober, Phys. Rev. E **56**, 427 (1997).
[41] S. Babuin, E. Varga, L. Skrbek, E. Lévêque, and P.-E. Roche, EPL Europhys. Lett. **106**, 24006 (2014); J. Salort, P.-E. Roche, and E. Lévêque, EPL **94**, 24001 (2011).
[42] The slight difference is rotational speed results from an attempt to reduce the axial component of the flow in the probe area.
[43] C. Simand, F. Chillà, and J.-F. Pinton, EPL Europhys. Lett. **49**, 336 (2000).